

**AFRL-DE-PS-  
TR-2007-1125**

**AFRL-DE-PS-  
TR-2007-1125**

---

## **Developing Pulsed Fiber Lasers**

**Steven Brueck**

**University of New Mexico  
Center for High Technology Materials  
1313 Goddard SE  
Albuquerque, NM 87106**

**15 June 2007**

**Final Report**

**APPROVED FOR PUBLIC RELEASE, DISTRIBUTION IS  
UNLIMITED**



**AIR FORCE RESEARCH LABORATORY  
Directed Energy Directorate  
3550 Aberdeen Ave SE  
AIR FORCE MATERIEL COMMAND  
KIRTLAND AIR FORCE BASE, NM 87117-5776**

---

DTIC COPY

## NOTICE AND SIGNATURE PAGE

Using Government drawings, specifications, or other data included in this document for any purpose other than Government procurement does not in any way obligate the U.S. Government. The fact that the Government formulated or supplied the drawings, specifications, or other data does not license the holder or any other person or corporation; or convey any rights or permission to manufacture, use, or sell any patented invention that may relate to them.

This report was cleared for public release by the Office of Public Affairs, 377<sup>th</sup> ABW, for Phillips Research Site and is available to the general public, including foreign nationals. Copies may be obtained from the Defense Technical Information Center (DTIC) (<http://www.dtic.mil>).

AFRL-DE-PS-TR-2007-1125 HAS BEEN REVIEWED AND IS APPROVED FOR PUBLICATION IN ACCORDANCE WITH ASSIGNED DISTRIBUTION STATEMENT.

//Signed//

//Signed//

---

MICHAEL L. VIGIL, DR-II  
Project Manager

---

WALLACE T. CLARK III, DR-IV  
Chief, Laser Division

This report is published in the interest of scientific and technical information exchange, and its publication does not constitute the Government's approval or disapproval of its ideas or findings.

# REPORT DOCUMENTATION PAGE

*Form Approved*  
*OMB No. 0704-0188*

Public reporting burden for this collection of information is estimated to average 1 hour per response, including the time for reviewing instructions, searching existing data sources, gathering and maintaining the data needed, and completing and reviewing this collection of information. Send comments regarding this burden estimate or any other aspect of this collection of information, including suggestions for reducing this burden to Department of Defense, Washington Headquarters Services, Directorate for Information Operations and Reports (0704-0188), 1215 Jefferson Davis Highway, Suite 1204, Arlington, VA 22202-4302. Respondents should be aware that notwithstanding any other provision of law, no person shall be subject to any penalty for failing to comply with a collection of information if it does not display a currently valid OMB control number. **PLEASE DO NOT RETURN YOUR FORM TO THE ABOVE ADDRESS.**

<b>1. REPORT DATE (DD-MM-YYYY)</b> 15-06-2007		<b>2. REPORT TYPE</b> Final Report		<b>3. DATES COVERED (From - To)</b> 01 Dec 2004 - 30 Sep 2007	
<b>4. TITLE AND SUBTITLE</b>  Developing Pulsed Fiber Lasers				<b>5a. CONTRACT NUMBER</b> FA9451-05-C-0163	
				<b>5b. GRANT NUMBER</b> N/A	
				<b>5c. PROGRAM ELEMENT NUMBER</b> 659901	
<b>6. AUTHOR(S)</b>  Steven Brueck				<b>5d. PROJECT NUMBER</b> Direct Cite	
				<b>5e. TASK NUMBER</b> N/A	
				<b>5f. WORK UNIT NUMBER</b> N/A	
<b>7. PERFORMING ORGANIZATION NAME(S) AND ADDRESS(ES)</b>  University of New Mexico Center for High Technology Materials 1313 Goddard S.E. Albuquerque, NM 87106				<b>8. PERFORMING ORGANIZATION REPORT NUMBER</b>	
<b>9. SPONSORING / MONITORING AGENCY NAME(S) AND ADDRESS(ES)</b>  Air Force Research Laboratory 3550 Aberdeen Ave., SE Kirtland AFB, NM 87117				<b>10. SPONSOR/MONITOR'S ACRONYM(S)</b>  AFRL/DELO	
				<b>11. SPONSOR/MONITOR'S REPORT NUMBER(S)</b>  AFRL-DE-PS-TR-2007-1125	
<b>12. DISTRIBUTION / AVAILABILITY STATEMENT</b> APPROVED FOR PUBLIC RELEASE, DISTRIBUTION IS UNLIMITED.					
<b>13. SUPPLEMENTARY NOTES</b> Appendix is a Masters Degree thesis draft for the work on this project by the Principal Investigator.					
<b>14. ABSTRACT</b> Laser power is at a premium and a diffraction limited optical beam delivers the maximum intensity on target. Therefore, the better the beam quality, the lower the system cost and complexity is reduced considerably by using high quality beams. Single mode optical fiber lasers and amplifiers produce near diffraction limited beams and therefore will result in near diffraction limited optical beams thus they will provide the highest intensities at the lowest laser powers. In the case of pulsed fiber lasers the factors that limit the output power are the fiber nonlinear effects and surface damage on the exit aperture. The nonlinear optical effects include Stimulated Brillouin Scattering (SBS), Stimulated Raman Scattering (SRS), self-phase modulation (SPM) and four-wave mixing (FWM) depending upon the application. For pulse durations of greater than 1-ns SPM and FWM can be neglected. The lowest threshold nonlinear process for long pulse duration is SBS. SBS can be effectively suppressed. The surface damage on the exit aperture can be eliminated by allowing free expansion in an "end cap" before the beam exits into free space.					
<b>15. SUBJECT TERMS</b> High Energy Pulsed Fiber Lasers					
<b>16. SECURITY CLASSIFICATION OF:</b>			<b>17. LIMITATION OF ABSTRACT</b>  SAR	<b>18. NUMBER OF PAGES</b>  40	<b>19a. NAME OF RESPONSIBLE PERSON</b> Michael L. Vigil
<b>a. REPORT</b> unclassified	<b>b. ABSTRACT</b> unclassified	<b>c. THIS PAGE</b> unclassified			<b>19b. TELEPHONE NUMBER (include area code)</b> 505 853 2914

**Standard Form 298 (Rev. 8-98)**  
Prescribed by ANSI Std. Z39.18



## TABLE OF CONTENTS

<u>Section</u>		<u>Page</u>
1.0	Introduction	1
2.0	Pulsed Amplifier Characterization Techniques	1
3.0	Development of Fiber Processing Skills and Techniques	2
4.0	Characterization of the Fibertek sub-ns Fiber Amplifier	3
5.0	Incoherent Beam Combination	4
6.0	Purchase of the Two Deliverable Hardware Items	5
7.0	Conclusions: Significant Accomplishments of the Research	5
8.0	Appendix: Apparent Incoherence Method	7



## **1.0 Introduction:**

Currently the Air Force has a significant need for high power, efficient, short pulse, compact laser systems. There are a number of potential Air Force applications of this technology, including illuminators and laser ranging systems. This research program has contributed to the advance in the state of the art of these laser systems by developing diagnostic tests for these systems. In addition, fiber laser fabrication skills were developed. The analysis and experimental design of a novel coherent beam combination system was performed. Finally, two phase modulators were delivered to AFRL.

Laser power is always at a premium and a diffraction limited optical beam delivers the maximum intensity on target. Therefore, the better the beam quality, the lower the system cost and complexity is reduced considerably by using high quality beams. Single mode optical fiber lasers and amplifiers produce near diffraction limited beams and therefore will result in near diffraction limited optical beams thus they will provide the highest intensities at the lowest laser powers. In the case of pulsed fiber lasers the factors that limit the output power are the fiber nonlinear effects and surface damage on the exit aperture. The nonlinear optical effects include Stimulated Brillouin Scattering (SBS), Stimulated Raman Scattering (SRS), self-phase modulation (SPM) and four-wave mixing (FWM) depending upon the application. The lowest threshold nonlinear process for long pulse duration is SBS. Whereas, for pulse durations of less than 1-ns SBS can be neglected, for these short pulse duration FWM, SPM and SRS are the effects that contribute to spectral broadening of the fiber laser system and may limit certain applications that require narrow linewidths. The output power limitation for a single mode pulsed fiber laser appears to be ~ 4-MW which is consistent with the 6-MW self-focusing limit observed in high quality bulk silica. The surface damage on the exit aperture can be eliminated by allowing free expansion in an “end cap” before the beam exits into free space.

## **2.0 Pulsed Amplifier Characterization Techniques**

The experimental procedures necessary to reliably characterize a pulsed fiber amplifier were investigated and developed. The measurements required are: 1) output power, 2) pulse Energy, 3) center wavelength, 4) spectral width of output, 5) beam quality ( $M^2$ ), 6) temporal pulse width.

A great deal of the time was devoted to understanding the measurement and pitfalls of using  $M^2$  to characterize the beam quality. During this quarter various techniques for making  $M^2$  measurements were explored and an experiment to measure the beam quality of a fiber amplifier was designed. A mathematical model was developed to model the cw performance of the pulsed amplifier that was being designed. Several variations in the design were examined.

Measurements of power, pulse energy, center wavelength, spectral width, and pulse width are significantly easier than beam quality. However, reliable characterization of a pulsed amplifier's performance still requires care in the design of the measurements. For

example, most optical power meters measure either pulsed energy at low repetition rate and average powers when the repetition frequency is increased. Since the pulsed amplifiers of interest are pumped by a continuous wave diode laser, it is necessary to operate the fiber amplifier at repetition rates of many kilohertz to prevent optical damage in the fiber amplifier.

Therefore some effort was expended to identify a fast pyroelectric joule meter that can be used to measure the energy in an individual pulse. Then an average power measuring device can measure the average power. It is necessary to measure the energy per pulse and the pulse repetition frequency to determine the average power in the pulses. By independently measuring the average power directly and then subtracting the energy per pulse time the repetition frequency from the measured average power, the amount of amplified spontaneous emission can be determined. A good amplifier will have very low amplified spontaneous emission. These two devices can be implemented easily to give accurate results. Similarly, an optical spectrum analyzer can be used to give the center wavelength and spectral width of the output. These instruments have been used for test measurements.

### **3.0 Development of Fiber Processing Skills and Techniques**

As part of this research effort Mr. Robin, the UNM graduate student, was developing the necessary fiber processing skills that are required for constructing and repairing fiber amplifiers. The main processes are as follows: 1) fiber fusion splicing, 2) fiber polishing, 3) adding connectors to optical fibers, and 4) fiber cleaving. Fiber cleaving is the process by which a glass optical fiber is cut such that a flat end surface is produced. Fiber fusion splicing is the process by which two fiber optic waveguides are precisely fused together. Two fiber ends are prepared by cleaving, which gives a clean flat surface for splicing. The two ends are then heated to the melting point of glass and pushed together. Fiber connectorizing is the process by which a fiber optic is held in a hardware connector. The connectors allow for easy implementation into optics bench experiments. After the fiber is placed in a connector it must be polished. In general, the input and output of a fiber optic must have a pristine surface for input and output of light. This is done with a spinning polishing disk. The connector is generally polished at an 8 degree angle to reduce reflections from the glass air interface; these allow higher gains to be achieved in the amplifier than are possible with flat uncoated fiber ends. The angle polishing of the glass to air interface reduces the optical feedback into the amplifier.

The output power from pulsed fiber amplifiers is often limited by optical surface damage at the air-glass interface. Endcapping is a technique that is used to increase the area of the output beam when it exits the glass. Endcapping is splicing a glass rod on the end of your amplifier output to allow the beam to propagate in glass outside a waveguide and expand. The power output of current fiber amplifiers requires that such endcapping techniques be employed. As the beam expands in the endcap the power per unit area decreases. Once this value is below the damage threshold of the air glass interface it can exit the fiber safely.

The construction of a pulsed amplifier based upon the modeling done in the previous quarter has begun. My amplifier will use ytterbium doped double clad fiber. The ytterbium is the gain material. It is pumped with a 976 nm diode, and produces stimulated emission at 1064 nm. A double clad fiber is a special design that allows the signal light to be guided in a ytterbium doped inner waveguide and the pump light guided in a non doped outer waveguide. The inner and outer waveguides are concentric. The nature of the outer waveguide requires that the guided 976nm light overlaps the doped inner waveguide, inverting the ytterbium ions. These fibers are defined by the size of the inner and outer waveguides. For example, the fiber used is 20/400, which is a 20  $\mu\text{m}$  doped core and a 400  $\mu\text{m}$  pump waveguide.

Currently there are two working fiber amplifiers. No testing has been done other than to measure output power. One amplifier has a maximum power output of 2.37 Watts and the other 5.77 W. The input pump power is in excess of 10 W. The second amplifier seems to have a reasonable output power. The first amplifier, however, is very low with respect to the amount of pump power.

This issue is related to the fusion splice between a “tapered fiber bundle” and the gain fiber. The “tapered fiber bundle” is a device which allows pump light to be injected into the cladding of the gain fiber, thus negating the need for free space optics coupling. A fiber coupled pump diode is fused to one leg of the “tapered fiber bundle” and then spliced to the gain fiber. This splice is lossy and does not allow some the signal light beyond the splice intersection.

The characterization of the pulsed fiber amplifier delivered to AFRL by a Fibertek began during this quarter. The chance to see how other people in the field build and test fiber amplifiers is good experience. The investigator, Mr. Craig Robin, learned a great deal about the details behind setting up an amplifier. For example, launching power into a fiber, or maximizing power output of an optical isolator.

#### **4.0 Characterization of the Fibertek sub-ns Fiber Amplifier**

Characterization of the pulsed amplifier delivered by a contractor was performed by us. Mr. Robin employed the experimental procedures developed for this characterization. Unfortunately, the amplifier broke while I was conducting measurements. The break occurred in one of the fibers in the amplifier. He was able to repair the damage with the fiber processing skills he acquired thus far.

The characterization of the amplifier has continued. The delivered fiber amplifier was unreliable and broke a number of times during the characterization process. In the process of repairing the contractor’s amplifier we learned a great deal about amplifier optimization and reliable design. For example, we learned that multiple modes will propagate down the fiber used in the delivered amplifier if the light is not properly launched into the fiber or if the fiber is mechanically disturbed even slightly. A single mode fiber waveguide provides the best possible beam quality and allows for an output beam of Gaussian intensity profile. The conditions of launched signal light can greatly effect the operation of an amplifier. If the light is launched into the fiber poorly, multiple

modes may propagate and energy extraction from the amplifier may be limited. None of these problems were emphasized by the contractor that delivered the pulsed fiber amplifier.

The amplifier was specified to have a less than 1-ns pulse duration with a spectral width of less than 30-GHz, a pulse energy of 1-mj, a repetition frequency of 10-kHz, and an  $M^2$  of less than 1.1. The amplifier had a 0.75-ns pulse duration, a 1.2-mj pulse energy, a 26-GHz linewidth, and a 12-kHz repetition frequency. The experimental procedure for beam quality measurement was developed, but it is necessary to reject the residual pump light exiting the pump cladding of the dual core fiber. Specifically, the  $M^2$  measurement requires that second moment of the beam intensity be measured. The second moment is an intensity weighted distance from the centroid of the beam. The second moment of a double clad fiber output is complicated by the fact that some light propagates in the outer cladding. The measurement is only concerned with the light in the core and it is impossible to distinguish between light originating in the core and light propagating in the cladding. This was overcome by collimating the signal beam and moving the Beam Master instrument approximately 4 feet from the laser output so that the intensity of the residual pump light was reduced to a negligible level compared to the signal intensity. The best beam quality measure produced an  $M^2 = 1.3$ .

Another idea related the pulsed amplifier work has been discussed. In general, we need a way to combine multiple amplifier outputs while maintaining good beam quality. Beam quality could be compromised during beam combination by coherent addition of the amplifier outputs. Thus an incoherent beam combination technique has been introduced.

Mr. Robin has completed the characterization of the delivered fiber amplifier, including beam quality. The culmination of all that I have learned about fiber amplifiers was used to basically re-build and test the delivered amplifier.

## **5.0 Incoherent Beam Combination**

Mr. Robin has turned his attention to the incoherent beam combination technique proposed by Dr. Shay. Dr. Shay has developed a model to describe the idea. In general, the technique requires the interfering fields be phase modulated. Mr. Robin generated a model using a separate premise which predicts certain behavior that is advantageous for incoherent beam combination. Both models predict the identical effects concerning the incoherent beam combination technique. The model equations were developed by hand, to gain considerable insight into the physics of this technique. This has led to a general understanding of multiple beam interference and how a phase modulation would affect that interference.

A Matlab class at UNM taught by Dr. Stephen Boyd significantly impacted my work in incoherent beam combination. Mr. Robin started to develop a Matlab code that basically repeats the work already done by Dr. Shay. Mr. Robin did this to practice his Matlab skills and also as a check to the model written by Dr. Shay. Thus far Mr. Robin found that Dr. Shay's results are consistent with his results. The original model

simplifies the problem slightly, and so Mr. Robin has accounted for all degrees of freedom in the problem. Even with the added degree of complexity the results remain consistent with Dr. Shay's original model.

With the model results in hand we designed initial experiments. The phase modulation and beam splitting were implemented in optical fibers. To check the incoherence of an individual pulse a gated camera with a gated window as short as several microseconds was used to test the concept.

A camera has been procured for the incoherent beam combination, and the remaining equipment necessary for the experiment was assembled. A fiber splitter was fused into the system to split the output from a single pulsed DBR laser into two fiber legs. The splitter takes a single fiber input and splits it into four outputs. The splitter is made out of three 2x2 3dB power splitters. After a couple attempts the splices appear to be consistent and the splitter demonstrates nearly equal power output from all legs.

An anamorphic prism pair was used to efficiently couple the elliptical Gaussian beam from the DBR laser into a single mode fiber.

The experimental effort on this contract halted on Feb. 24, 2006 when the graduate student, Mr. Craig Robin, was hired by AFRL as a civilian government employee.

## **6.0 Purchase of the Two Deliverable Hardware Items**

Two EO Space Model SP-1x8-PH-VA-PFU-PFU-106-S, Lithium Niobate 1x8 Polarization Maintaining Splitter with Integrated Phase and Amplitude controls were ordered and received. These items are contract deliverable items and are being delivered to AFRL as required in the contract.

## **7.0 Conclusions: Significant Accomplishments of this Research**

In this research effort, we developed techniques for characterizing the performance of state-of-the-art pulsed fiber lasers that demonstrated world record performance. A number of fiber processing techniques needed to build MW peak power fiber lasers were developed as well as pulsed fiber design skills. Additional modeling of a novel incoherent beam combination method was performed and the first demonstration experiment was designed.

The graduate student who performed the research under this contract was hired as a Civil Servant at the Air Force Research Laboratory. Additional contributions include the support of Mr. Craig Robin at the beginning of his graduate research; he expects to defend his MS thesis summer 2007.

This research contributed to the 2 presentations at the 20<sup>th</sup> Solid State and Diode Laser Technology Review, Los Angeles, CA, June 26-28, 2007, the titles of the presentations are listed below:

1. "A Novel Scintillation Suppression Technique," Thomas M. Shay, Craig Robin, Lt. Justin Spring, and Athanasios Gavrielides.
2. "Theoretical Description of a Novel Scintillation Suppression Technique," Thomas M. Shay, Craig Robin, Lt. Justin Spring, and Athanasios Gavrielides.

Finally, the purchase and delivery of two EO-Space phase modulators was accomplished as the final task.

# Apparent Incoherence Method

## Appendix

### Table of Contents

<u>Section</u>	<u>Page</u>
1.0 Introduction	9
2.0 Theory	17
2.1 Apparent Coherence Factor with N Electric Fields	17
2.2 2 Legs – One Leg Phase Modulated & One Leg without Phase Modulation	24
2.3 Multiple Legs Phase Modulated	30
3.0 Experimental Results	31
4.0 Conclusion	32

## List of Figures

<u>Figure</u>	Page
Figure #1: Experimental setup for hologram creation on photographic film using a moving diffuser to reduce image speckle.	10
Figure #2: Schematic diagram of the laser diode microscope with an illuminating light coming from a single mode diode with optical feedback coupled into a multimode fiber.	12
Figure#3: The moving aperture method of reducing speckle the reconstructed image is re-imaged by a lens with a moving aperture inside the fixed pupil; it is understood that the fixed pupil matches the pupil of the reconstructed image plane hologram.	13
Figure#4: Scintillation can be further reduced by exploiting the spatial diversity present in turbulent optical channels.	15
Figure#5: Apparent coherence factor vs. experiment for a pulsed fiber system with pulse duration of 25 $\mu$ sec.	32

## 1.0 Introduction

Speckle and scintillation have been limiting factors in information transfer with coherent light sources since the advent of the laser. Speckle is the mottled light intensity pattern that results when a laser is reflecting off a non-specular surface. In an imaging system the mottled intensity pattern overlays the actual image and degrades quality.

Scintillation causes fluctuations in laser beam power which are a result of a transverse phase variations in the wavefront. This effect is commonly encountered in atmospheric laser propagation. The atmosphere can be seen as being made up of many small pockets of turbulent air, each having slightly different refractive index properties. As a laser beam propagates these pockets act as weak lenses which deflect the light slightly and cause random transverse path length differences, giving rise to temporally varying interference. In a free space laser communications system this interference is seen by a detector system as a power fluctuation.

These phenomena are a result of the coherent nature of laser light, and are inherent to any system employing a coherent source. A handful of techniques have been devised to overcome these limitations.[1] These methods of speckle and scintillation mitigation will be discussed in relation to image processing and free space optical communications systems (FSO). The solutions are generally classified into five categories: 1) control of spatial coherence, 2) control of temporal coherence, 3) spatial sampling, 4) spatial averaging, 5) digital image processing. A sixth method is proposed herein which we have named Apparent Incoherence Method (AIM).

The control of spatial coherence requires a temporal average of multiple speckle patterns collected by a detector. The technique relies on the averaging characteristic of a detectors finite response time. What is left to the experimenter is then is to change the speckle pattern

sufficiently over the duration of this response time, thus washing out the non-uniform illumination. An early example of this method was demonstrated by De Bitteto[2] who showed that laser light passing through a diffuser, like a moving ground glass plate, reduced speckle produced on photographic film. A random phase plate creates a large number of path length differences in the transverse extent of the beam such that the intensity fluctuations occur on a very small scale. Rotation of the phase plate shifts the position of these fluctuations so as to be averaged by the detection system. Figure 1 below is the experimental setup from De Bitteto's work.

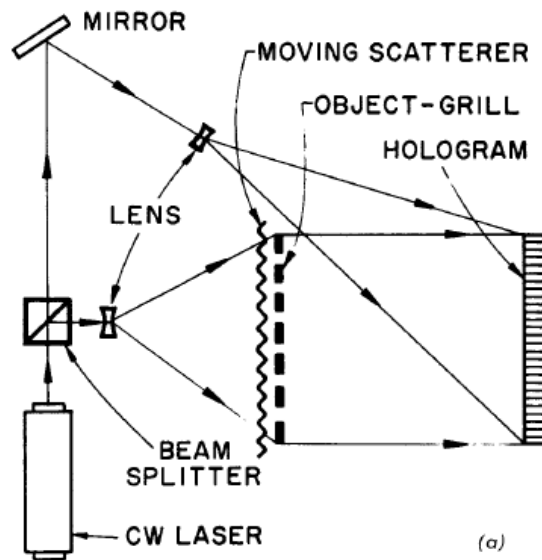


Figure 1: Experimental setup for hologram creation on photographic film using a moving diffuser to reduce image speckle.

More recent work, done by Lai [3], in the control of spatial coherence uses the same technique of rotating a diffuser, but instead employs a holographic phase plate. The phase plate allows one to maintain beam quality and laser brightness by introducing a small diffusing angle, while removing speckle.

Techniques for the control of spatial coherence remain unchanged over the past 40 years, and work well for specific applications, such as imaging, when the detector system is allowed to have a very small bandwidth. The bandwidth limitation is a product of the mechanically moving diffuser required in spatial coherence control techniques.

Speckle and scintillation may also be mitigated in part through the control of the temporal coherence of the laser source. In general this is done by time averaging the speckle patterns produced by multiple wavelengths of light. This can be thought of as using multiple lasers in signal transfer, or using a single laser with a large spectral bandwidth. George and Jain derived an expression for the wavelength spacing required to decouple the speckle patterns arising from two monochromatic tones in an imaging system.[4] They also demonstrated a reduction in speckle due to the averaged speckle patterns from six monochromatic lines emitted from a carbon arc lamp. The plurality of frequencies contained in the source is exploited to give rise to coherent combinations, which change so fast over the spatial extent on the beam, that the detection system time averages the signal making it seem incoherent.

Later, Dingel and Kawata provide feedback into a single mode diode laser which causes multimode operation.[5] The effect of multiple longitudinal modes reduces the coherence length of the illuminating laser. The output of the laser diode is then passed through a multimode fiber whose exit face illuminates a conventional microscope with a continuously changing speckle

pattern. These uncorrelated speckle patterns are averaged by a video detector to reduce speckle noise. Figure 2 below shows the experimental setup.

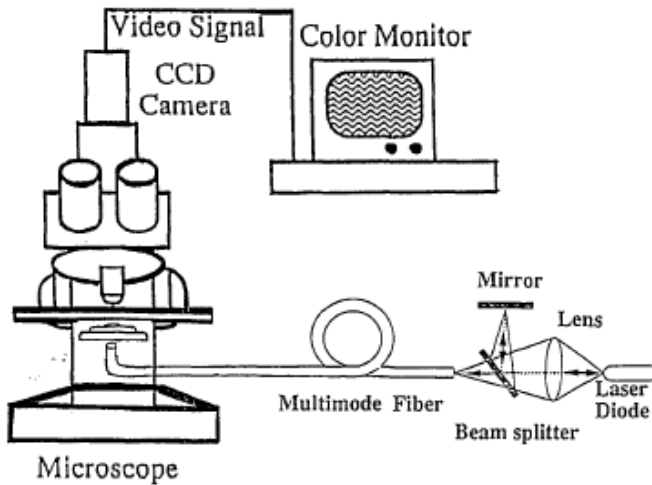


Figure 2: Schematic diagram of the laser diode microscope with an illuminating light coming from a single mode diode with optical feedback coupled into a multimode fiber.

Temporal coherence control techniques do not suffer from the bandwidth limitations found in spatial control of coherence, however the applications are still limited. The effective mechanism in all temporal control techniques is an increase in spectral bandwidth resulting in a decrease in coherence length. This is not a problem when the signal receiving system accepts a large bandwidth of light. A FSO system, for example, would require a source which is very narrow in frequency space, and a detector with a matching bandwidth with the intention of increasing signal to noise response. Issues with scintillation and speckle could not be mitigated for this application without a decrease in signal fidelity.

Spatial sampling was, initially, one of the most popular speckle reduction techniques, first presented by Dainty and Welford. [6] In general, the illuminating light is sampled from a laser by a moving aperture. The effect is a constantly changing phase relationship which is time average by the detector. Figure 3 below shows how the speckle generated in the creation of a hologram can be removed by a moving pupil imaging system.

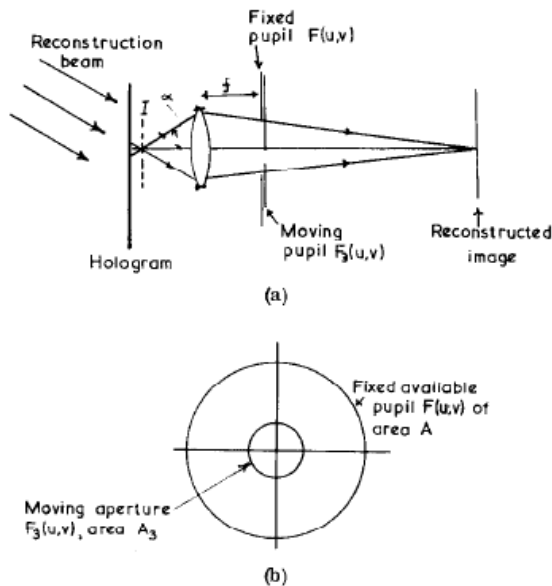


Figure 3: The moving aperture method of reducing speckle the reconstructed image is re-imaged by a lens with a moving aperture inside the fixed pupil; it is understood that the fixed pupil matches the pupil of the reconstructed image plane hologram.

Y. Kawagoe et al. furthered the research in the early 80's by using a rotating aperture at the Fourier transform plane of the object. [7] The moving aperture technique was supplanted by other speckle reduction techniques and is not a current area of research.

Spatial averaging considers the size of individual speckles in a speckle pattern. In an imaging system these speckles may be washed out if their size is smaller than the system

resolution. However, when this is not the case, e.g. speckle size is larger than an element in a CCD camera, information is lost. Iwai et al. theoretically and experimentally investigate speckle statistics as a function of detector aperture size and integration time. [8] They show speckle pattern change was inversely related to aperture size, or the time varying change in speckle patterned decreased with aperture size.

Currently the most popular method of speckle reduction for FSO is aperture averaging. Unlike an imaging system, a free space laser communications system only needs to capture the transmitted light. Scintillation produces an irradiance pattern that is random in both space and time at the detector. An optical receiver with a very small aperture will produce a random signal. If the aperture is larger than the spatial scale of the irradiance fluctuations, the receiver will average fluctuations over the aperture, and the signal fluctuations will be less than those from a point receiver. [9] This solution also has limitations. Scaling aperture size is costly and often times inconvenient. Furthermore, the intensity fluctuations are constantly changing in the aperture and therefore constantly changing at the detector plane. If the detecting element is not large enough the focused spot may move off the detector, a phenomena referred to as fading. Since free space laser communication is only practical if GHz bandwidths are accessible there is a limit to detector size. Anguita et al. simulate a reduction in scintillation effects with a combination of aperture averaging and multiple signal transmission elements. [10] This arrangement exploits the effect of scintillation causing a higher density speckle pattern at the receiver due to the overlap of speckle patterns from each element, in essence a reduction in spatial coherence. Figure 4 is a concept diagram of the system.

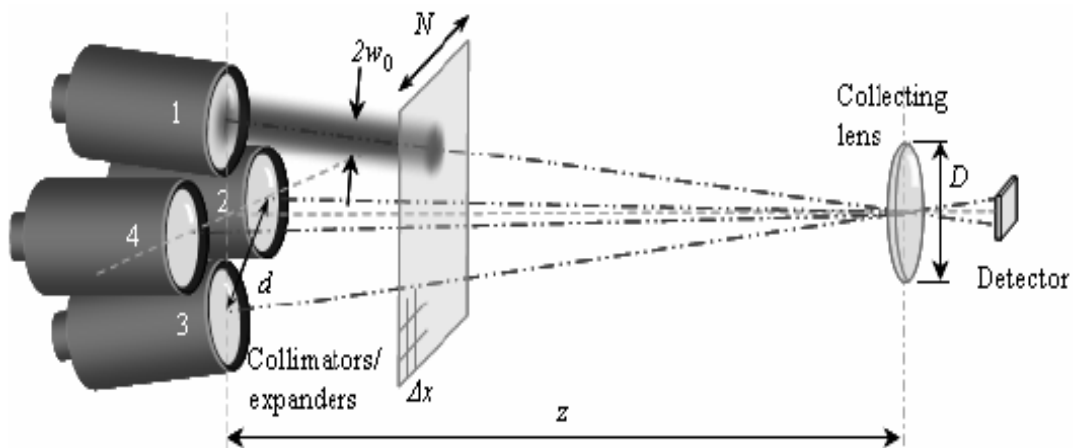


Figure 4: Scintillation can be further reduced by exploiting the spatial diversity present in turbulent optical channels.

The increase in computing power has allowed digital image processing techniques to be developed for speckle reduction. The shift from hardware to software was also motivated by the development of fast wavefront sensors and manipulators. An imaging system generally requires speckle reduction created by very small wavefront variations in the system itself. These variations are too small to be compensated by current wavefront sensor technology. As an example digital speckle pattern interferometry (DSPI) is an entire field optical method for non-contact and nondestructive surface analysis. [11] Specific digital image processing algorithms are used to reduce speckle patterns overlaying images.

FSO systems employing digital signal processing generally rely on a wavefront detection scheme and then an optimization metric to manipulate the source and compensate for the atmospheric turbulence. The process solves the problem of scintillation by applying the inverse of the wavefront distortion obtained in signal propagation. This specific technology is often

limited related to the speed at which the wavefront correction system can be adjusted. Also the method is slowed by the computer algorithm used to dissect each the aberrant wavefront. [12]

The techniques described above generally effect the spatial or temporal coherence of the source or modify the method of detection. In general, the focus is on the transmitting or receiving part of the system. Anguita attempts to marry two technologies, one effecting the transmitter and the other effecting the detector, but the two are not correlated. Table 1 below summarizes these methods for speckle an scintillation reduction and includes AIM.

<b>1.1.1 Technique</b>	<b>1.1.2 Area of Use</b>	<b>1.1.3 Comments</b>
Apparent Incoherence Method	Information Processing/ Free Space Optics	Effects only temporal coherence
Control of Spatial Coherence	Information Processing	Bandwidth limited due to mechanically moving parts
Control of Temporal Coherence	Information Processing	Requires spectrally broad source
Spatial Sampling	Information Processing	Requires moving aperture
Spatial Averaging	Information Processing/ Free Space Optics	Requires aperture scaling
Digital Image Processing	Information Processing/ Free Space Optics	Computationally rigorous which decreases bandwidth

Table 1: A summary of speckle and scintillation reduction techniques, including Apparent Incoherence Method. The comments are indication possible limitations.

The apparent incoherence method correlates the integration time of the detection system to a phase modulation put on the transmitter. The system described here uses a narrow linewidth source which is split into two legs. One leg is phase modulated at a frequency  $1/\tau$  where  $\tau$  is the

pulse duration, while the other is left un-modulated. The two legs are brought back together to interfere at the detector. When the phase modulation amplitude is selected to be at a zero of the Bessel function of the first kind of order zero and the product of the phase modulation frequency times the pulse duration are properly selected then the time averaged signal at the photodetector appears to be the result of incoherent combination. Beam break up due to wavefront distortions in transmission through the atmosphere will not be compensated for by AIM. Interference fringes of a single pulse will be swept across a detector at the focal plane of the receiving aperture leading to a time average intensity equivalent to that of incoherent illumination.

## 2 2.0 Theory

### 2.1 Apparent Coherence Factor with N Electric Fields

In general, the combination of N electric fields will produce a resultant field that is the sum of the individual fields. The instantaneous intensity of these combined fields is defined as,

$$I(t) = \sqrt{\frac{\epsilon_o}{\mu_o}} \cdot |(E_N(t_N))|^2 = \sqrt{\frac{\epsilon_o}{\mu_o}} \cdot \sum_{i=1}^N \sum_{\substack{j=1 \\ j \neq i}}^N \left[ |E_i(t_i)|^2 + (E_i(t_i)) \cdot E_j(t_j) \right] \quad , \text{Eq. 1}$$

where  $D_i$  is the optical path length from the  $i^{\text{th}}$  source to the observation point and  $E_i(t)$  represents the independent fields. The second term on the right hand side of Eq. 1 is the cross term between the different contributing fields gives rise to the interference that causes fringes. The  $i^{\text{th}}$  electric field can be expressed by a cosine,

$$E_i(t) = A_i(t_i) \cdot \text{Cos}(\omega_i(t_i) \cdot t_i - \phi_i) \quad ,\text{Eq. 2}$$

where  $A_i(t_i)$  represents the real field amplitude (that can vary with time, such as in a pulsed source),  $\omega_i(t_i)$  represents source frequency (that again can vary with time, such as in a chirped source), and  $\phi_i$  represents the phase shift accumulated by the  $i^{\text{th}}$  optical field as it travels from the source to the observation point. When the electric field is expressed in real terms like Eq. 2, than Eq. 1 can be simplified to,

$$I(t) = \sqrt{\frac{\epsilon_o}{\mu_o}} \cdot \sum_{i=1}^N \sum_{\substack{j=1 \\ j \neq i}}^N \left[ \begin{aligned} & \frac{A_i(t_i)^2}{2} (1 + \text{Cos}[2\omega_i(t_i) \cdot t_i - 2\phi_i]) \\ & + A_i(t_i) A_j(t_j) \left\{ \begin{aligned} & \text{Cos}[(\omega_i(t_i) \cdot t_i + \omega_j(t_j) \cdot t_j) - (\phi_i + \phi_j)] \\ & + \text{Cos}[(\omega_i(t_i) \cdot t_i - \omega_j(t_j) \cdot t_j) - (\phi_i - \phi_j)] \end{aligned} \right\} \end{aligned} \right] \quad ,\text{Eq. 3}$$

where,  $\mu_o$  and  $\epsilon_o$  represent the magnetic and electric permeabilities of free space. Electronic photodetectors can not follow optical frequencies. Terms in Eq. 3 that oscillate at optical frequencies do not contribute to the measured signal and can be neglected. Therefore the signal detected is proportional to the terms below,

$$I(t) = \sqrt{\frac{\epsilon_o}{\mu_o}} \cdot \sum_{i=1}^N \sum_{j=i+1}^N \left[ \frac{A_i(t_i)^2}{2} + A_i(t_i) A_j(t_j) \cdot \left\{ \text{Cos}[(\omega_i(t_i) \cdot t_i - \omega_j(t_j) \cdot t_j) - (\phi_i - \phi_j)] \right\} \right] \quad ,\text{Eq. 4}$$

If the beat frequencies  $(\omega_i - \omega_j)$  are much greater than the detector bandwidth, then the cosine frequency difference term time averages to zero, and the illumination appears incoherent.

However, if a single optical beam is divided into two or more optical paths and then recombined the following simplification can be made to Eq 4. We see from Eq 5, that the interference term depends only upon the phase differences between the different paths. The second term in the

sum is the interference term that gives rise to the phase dependent intensity variations for coherent beams,

$$I(t) = \sqrt{\frac{\epsilon_o}{\mu_o}} \cdot \sum_{i=1}^N \sum_{j=i+1}^N \left[ \frac{A_i(t_i)^2}{2} + A_i(t_i) A_j(t_j) \cdot \text{Cos}[(\phi_j - \phi_i)] \right] \quad ,\text{Eq. 5}$$

A coherent beam combination scheme would use a multiple output system, and nominally equal optical paths lengths in all legs. The desired effect is an output beam with spatial intensity characteristics which remain constant in time. Phase differences  $\phi_i - \phi_j$  will vary randomly in time due to changes in the environment. The physical path lengths must be matched and made stable by compensating for these environmental effects, for the measured spatial intensity pattern of the combined beams to remain constant. In general, any method of coherent beam combination requires a very complex and expensive system to dynamically compensate for random phase variations.

With no compensation, random phase variations due to environmental changes can be significant, even in a bench top experiment. Applications that require beam propagation through the atmosphere undergo considerable phase distortion, much of which is caused by scintillation. As phase differences change in time so will spatial intensity patterns. Under these conditions, the intensity projected will be highly non-uniform and will vary from very bright to zero intensity. Furthermore, the bright and dark spot positions vary in time in an unpredictable way. For a large number of applications these dark spots are unacceptable, and can represent a loss of information. Mathematically we avoid the random coherent combination of the output beam by controlling the phase difference in the cross term in Eq. 5, or making entire cross term go to zero.

A novel incoherent beam combination method for measuring spatially uniform illumination patterns is described. There are many methods for achieving a uniform illumination pattern via incoherent beam combination; one of the simplest being to change the optical path length of the various legs until the coherence length is exceeded, rendering the combined sources incoherent. This method is not described above mathematically, as we have not included coherent sources with a finite spectral width. The drawback to this method is the source is required to have a spectrally wide bandwidth for a practical implementation. A wide bandwidth source is not desirable if a signal transmission and detection application is intended. An increase in spectral bandwidth results in a lower signal to noise ratio. Furthermore, if the source is pulsed, path lengths must be matched to ensure that the pulses temporally overlap when reaching their final target. For nearly transform limited coherent sources with short pulse widths, the required path length mismatch for achieving incoherence is very often greater than or a large fraction of the pulse duration, thus this technique has limited applicability. In addition, narrow linewidth sources, pulsed or continuous wave (CW), may have a very long coherence length. This can make having a path length mismatch greater than this large coherence length inconvenient, again making another solution attractive. Finally, there are also a significant number of important applications where the optical path lengths can not be controlled. The technique described in this patent provides a unique solution to those problems.

The solution introduced here is to independently phase modulate each leg, so that  $\phi_i$  and  $\phi_j$  are no longer constant in time and can be expressed at the observation point as,

$$\phi_i(t) = \phi_{i0} + \beta_i \cdot \text{Sin}[\omega_{RF-i} \cdot t_i + \xi_{RF-i}] \quad ,\text{Eq. 6}$$

where  $\phi_{i0}$  is the time-independent initial phase offset term,  $\beta_i$  is the modulation amplitude,  $\omega_{RF-i}$  is the frequency of the introduced phase modulation on the  $i^{\text{th}}$  leg, and  $\xi_{RF-i}$  is the initial phase of the phase modulation apparatus.

When  $\phi_i$  and  $\phi_j$  vary with time, interference fringes still exist, and the spatial intensity pattern is also a function of time. When the phase modulation of  $\phi_i$  and  $\phi_j$  is faster than the integration time of the detector being used or the pulse duration, whichever is shorter, then the fringes will move so quickly they will be averaged by the detector and produce a signal equivalent to incoherent combination, providing that the modulation is properly performed. This is the intuitive picture of incoherent beam combination due to phase modulation. Substituting Eq. 6 into Eq. 5,

$$I(t) = \sqrt{\frac{\epsilon_o}{\mu_o}} \cdot \sum_{i=1}^N \sum_{j=i+1}^N \left[ \begin{array}{l} \frac{A_i(t_i)^2}{2} + A_i(t_i) A_j(t_j) \cdot \\ \text{Cos} \left( \begin{array}{l} \phi_{j0} - \phi_{i0} - \beta_i \cdot \text{Sin}[\omega_{RF-i} \cdot t_{RF-i} + \xi_{RF-i}] \\ + \beta_j \cdot \text{Sin}[\omega_{RF-j} \cdot t_{RF-j} + \xi_{RF-j}] \end{array} \right) \end{array} \right] \quad , \text{Eq. 7}$$

Eq. 7 shows the instantaneous intensity, however, we are more interested in the time averaged intensity, as that is the signal produced by the detector. The calculation below shows the time averaged intensity where  $\tau$  represents the integration time of the detector or the pulse duration.

$$I_{Ave} = \left\{ \begin{array}{l} \sqrt{\frac{\epsilon_o}{\mu_o}} \cdot \\ \frac{1}{\tau} \int_T^{T+\tau} \left[ \sum_{i=1}^N \sum_{j=i+1}^N \left[ \begin{array}{l} \frac{A_i(t_i)^2}{2} \\ + A_i(t_i) A_j(t_j) \cdot \text{Cos} \left( \begin{array}{l} \phi_{j0} - \phi_{i0} + \beta_i \cdot \text{Sin}[\omega_{RF-i} \cdot t_{RF-i} + \xi_{RF-i}] \\ - \beta_j \cdot \text{Sin}[\omega_{RF-j} \cdot t_{RF-j} + \xi_{RF-j}] \end{array} \right) \end{array} \right] \right] \cdot dt \end{array} \right\} \quad \text{Eq. 8}$$

where T represents the time when the integration begins. The second term in the summation is the interference term which is zero for incoherent beam combination and gives rise to the spatial intensity variations in the illumination pattern.

Eq. 8 can be separated into the term that is common to both coherent and incoherent beam combination,

$$I_{Ave\_Inc} = \sqrt{\frac{\epsilon_o}{\mu_o}} \cdot \frac{1}{\tau} \int_T^{T+\tau} \left( \sum_{i=1}^N \left[ \frac{A_i(t_i)^2}{2} \right] \right) dt \quad ,Eq. 9$$

the second term in the summation in Eq. 8 term that gives rise to the interference and is unique to the superposition of coherent beams,

$$\Delta I_{Ave} = \left\{ \sqrt{\frac{\epsilon_o}{\mu_o}} \cdot \frac{1}{\tau} \int_T^{T+\tau} \left[ \sum_{i=1}^N \sum_{j=i+1}^N \left[ A_i(t_i) A_j(t_j) \cdot \text{Cos} \left( \begin{array}{l} \phi_{j0} - \phi_{i0} + \beta_i \cdot \text{Sin}[\omega_{RF-i} \cdot t_{RF-i} + \xi_{RF-i}] \\ -\beta_j \cdot \text{Sin}[\omega_{RF-j} \cdot t_{RF-j} + \xi_{RF-j}] \end{array} \right) \right] \right] \cdot dt \right\} ,Eq.10$$

this is the coherent interference term that gives rise to intensity fluctuations in the illumination pattern. In the absence of phase modulation,  $\Delta I_{Ave}$  represents the change in the measured intensity as the optical phases are varied. When the modulation amplitudes for all of the fields are set equal to zeros of the Bessel function of the first kind of order zero, and the field amplitudes are all equal, then it is possible to find sets of modulation frequencies where the detected intensity fluctuations due to interference between the fields is indistinguishable from an

incoherent intensity pattern. Under those conditions,  $\Delta I_{Ave}$ , the second summation in the integral in Eq. 8 averages to zero, leaving only the incoherent term.

As a convenient metric for evaluating the degree of apparent coherence, we define the Apparent Coherence Factor (ACF), as the ratio of the maximum magnitude of the interference term as the optical and RF phases are varied,  $\Delta I_{Ave\_max}$ , to the magnitude of the incoherent term

$$ACF = \frac{|\Delta I_{Ave\_max}|}{I_{Ave\_Inc}} \quad ,Eq. 11$$

The ACF for perfectly coherent fields has an upper limit of unity while the ACF for perfectly incoherent fields is zero. The ACF defines the worse case performance for a given set of modulation amplitudes, modulation frequencies, and integration time.

Substituting for  $I_{Ave\_Inc}$  and  $\Delta I_{Ave}$  in Eq. 11 using Eqs. 9 and 10 we obtain,

$$ACF = \frac{\left| \frac{1}{\tau} \int_T^{T+\tau} \left[ \sum_{i=1}^N \sum_{j=i+1}^N \left[ A_i(t_i) A_j(t_j) \cdot \text{Cos} \left( \begin{array}{l} \phi_{j0} - \phi_{i0} + \beta_i \cdot \text{Sin}[\omega_{RF-i} \cdot t_{RF-i} + \xi_{RF-i}] \\ -\beta_j \cdot \text{Sin}[\omega_{RF-j} \cdot t_{RF-j} + \xi_{RF-j}] \end{array} \right) \right] \right] \cdot dt \right|}{\left| \frac{1}{\tau} \cdot \int_T^{T+\tau} \sum_{i=1}^N \left[ \frac{A_i(t_i)^2}{2} \right] \cdot dt \right|} \quad ,Eq.12$$

where the apparent coherence is the coherence averaged over a the time interval,  $\tau$ . When there is no RF phase modulation, the ACF is zero for perfectly incoherent light and has an upper limit of unity for perfectly coherent light. Ideally the ACF is independent of the optical phase differences and the RF phase differences, indeed these conditions exist for a two leg system.

However, for most multi-phase modulated systems, it is necessary to use Eq. 12 to calculate the

ACF. A worse case value for the ACF can be calculated for a given integration time,  $\tau$ , RF frequencies,  $\omega_{RF-i}$ , and phase modulation amplitudes,  $\beta_i$ . Calculating the ACF for all possible values of the optical and RF starting phases will give an upper limit on the Apparent Coherence Factor.

The experimental design parameters that are accessible for minimizing the apparent incoherence factor are; the phase modulation amplitude,  $\beta_i$ 's, the phase modulation frequencies,  $\omega_{RF-i}$ 's, and integration time,  $\tau$  (though in practical applications  $\tau$  is less likely to be an adjustable parameter than frequency and beta). Thus, the intensity fluctuations due to coherent combination can be minimized by adjusting those design parameters to minimize the apparent incoherence factor, ACF, in Eq. 12. Then Eq. 12 can be used to place an upper limit on the residual intensity fluctuations due to interference effects.

## 2.2 2 Legs – One Leg Phase Modulated & One Leg without Phase Modulation

The apparent coherence factor for a two leg system excited by a common coherent source, with one leg phase modulated and one leg unmodulated, can be calculated using Eq. 12 by setting N equal to 2 and  $\beta_2$  equal to zero. It is important to note that the two leg system is the only apparent incoherence method system where optimum performance can be achieved without phase modulating all of the legs. Then, for this two leg system, Eq. 12 simplifies to,

$$ACF = \left| \frac{\frac{1}{\tau} \int_T^{T+\tau} \left[ A_1(t_1) A_2(t_2) \cdot \text{Cos}(\phi_{20} - \phi_{10} + \beta_1 \cdot \text{Sin}[\omega_{RF-1} \cdot t_{RF-1} + \xi_{RF-1}]) \right] \cdot dt}{\frac{1}{\tau} \int_T^{T+\tau} \left[ \frac{A_1(t_1)^2}{2} + \frac{A_2(t_2)^2}{2} \right] \cdot dt} \right| \quad , \text{Eq. 13}$$

The denominator represents the incoherent field addition, while the numerator represents interference effects. To minimize the coherence effects the experimental parameters must be adjusted so that the ACF is within acceptable limits. Ideally, the ACF should integrate to zero for arbitrary optical phase differences,  $\phi_{20}-\phi_{10}$ , and for arbitrary RF phases,  $\xi_{RF-1}$ . Thus the ideal situation occurs when the numerator of the ACF is zero,

$$ACF_{Num} = \left\{ \frac{1}{\tau} \int_T^{T+\tau} \left[ A_1(t_1) A_2(t_2) \cdot \cos(\phi_0 + \beta_1 \cdot \sin[\omega_{RF-1} \cdot t_{RF-1} + \xi_{RF-1}]) \right] dt \right\} = 0 \quad ,Eq. 14$$

where  $\phi_0 = \phi_{20} - \phi_{10}$  combines the two independent optical phases that can vary from pulse to pulse and  $ACF_{Num}$  represents the numerator of the ACF. The numerator of the ACF is proportional to the interference effect amplitudes, therefore when that is zero the interference effects are eliminated over the integration time of the detector.

Solely for the purpose of teaching the principles of the Apparent Incoherent Method, a few simplifying assumptions will be made. Assuming that field amplitudes are square pulses in time, the detector integration time is greater than the pulse duration,  $\tau$ , and that the pulses from the different path lengths are temporally synchronous, so that  $\frac{|L_1 - L_2|}{c} \ll \tau$ , where  $L_1$  and  $L_2$  represent the path lengths of the two legs and  $c$  represents the speed-of-light in the medium. These assumptions are made only to clarify the basic principles involved. Under those assumptions, we can rewrite Eq. 14,

$$ACF_{Num\_sq} = \left\{ A_1 \cdot A_2 \cdot \frac{1}{\tau} \int_T^{T+\tau} \cos(\phi_0 + \beta_1 \cdot \sin[\omega_{RF-1} \cdot t_{RF-1} + \xi_{RF-1}]) dt \right\} ,Eq. 15$$

where  $ACF_{Num\_sq}$  is proportional to the strength of the interference term for the square pulses.

When  $ACF_{Num\_sq}$  integrates to zero then the photodetector measures a signal that is identical to the signal generated by an incoherent signal even if the different beam paths are derived from a single master oscillator with a very narrow linewidth. Using the cosine sum angle identity Eq.

15 is rewritten,

$$ACF_{Num\_sq} = \left\{ \frac{A_1 \cdot A_2}{\tau} \int_T^{T+\tau} \left\{ \begin{array}{l} \text{Cos}(\phi_0) \cdot \text{Cos}(\beta_1 \cdot \text{Sin}[\omega_{RF-1} \cdot t_{RF-1} + \xi_{RF-1}]) \\ -\text{Sin}(\phi_0) \cdot \text{Sin}(\beta_1 \cdot \text{Sin}[\omega_{RF-1} \cdot t_{RF-1} + \xi_{RF-1}]) \end{array} \right\} dt \right\}, \text{Eq. 16}$$

Replacing the time dependent terms in Eq. 16 by their respective Fourier Series Eq. 16 can be written in the following form,

$$ACF_{Num\_sq} = \left[ \frac{A_1 \cdot A_2}{\tau} \int_T^{T+\tau} \left\{ \begin{array}{l} \text{Cos}(\phi_0) \cdot \left[ \begin{array}{l} J_0(\beta_1) \\ +2 \cdot \sum_{n=1}^{\infty} \left[ \begin{array}{l} J_{2n}(\beta_1) \cdot \\ \text{Cos}(2n \cdot (\omega_{RF-1} \cdot t_{RF-1} + \xi_{RF-1})) \end{array} \right] \end{array} \right] \\ -\text{Sin}(\phi_0) \cdot \left[ \begin{array}{l} 2 \cdot \sum_{n=1}^{\infty} \left[ \begin{array}{l} J_{2n-1}(\beta_1) \cdot \\ \text{Sin}((2n-1)(\omega_{RF-1} \cdot t_{RF-1} + \xi_{RF-1})) \end{array} \right] \end{array} \right] \end{array} \right\} dt \right], \text{Eq. 17}$$

For the superimposed pulses to appear to be incoherent for every pulse regardless of the optical phase difference the integral of each individual term of Eq. 17 must integrate to zero. The other possibility is that individual terms are nonzero but cancel each other. However, that is not a general case because  $\phi_0$  and  $\xi_{RF-1}$  are random phase terms. If there were nonzero terms that did cancel each other it would partly be a result of these random phase terms, meaning that the next time the experiment is carried out it would be very likely that new random phases would be

encountered, eliminating the cancellation. In the worse case, the fringes would blink on and off from pulse to pulse.

Experimentally, one would want to impose conditions that made each individual term integrate to zero regardless of the random phases. Two parameters in Eq. 19, are easily controlled experimentally,  $\beta$  and  $\omega_{RF-1}$ . The only means of zeroing the non time dependent term in Eq. 17 is to set  $\beta$  equal to a zero of  $J_0$ . Ideally the integral of the other terms in Eq. 17 should also be zero. Rigorously, this means that conditions must be adjusted so that the following equalities are true,

$$\frac{1}{\tau} \int_T^{T+\tau} \text{Cos}(2n \cdot (2\pi \cdot f_{RF-1} \cdot t_{RF-1} + \xi_{RF-1})) dt = 0$$

and

$$\frac{1}{\tau} \int_T^{T+\tau} \text{Sin}((2n-1) \cdot (2\pi \cdot f_{RF-1} \cdot t_{RF-1} + \xi_{RF-1})) dt = 0$$

, Eqs. 18a-c

$$\text{where....} f_{RF-1} = \frac{\omega_{RF-1}}{2\pi}$$

Eqs. 18 a and b have the exact analytical solutions given below,

$$\frac{1}{\tau} \int_0^{\tau} \text{Cos}(2n \cdot (2\pi \cdot f_{RF-1} \cdot t_{RF-1} + \xi_{RF-1})) dt =$$

$$\frac{\text{Cos}(2 \cdot n \cdot (\xi_{RF-1} + \pi \cdot f_{RF-1} \cdot \tau)) \cdot \text{Sin}(2 \cdot n \cdot \pi \cdot f_{RF-1} \cdot \tau)}{2 \cdot n \cdot \pi \cdot f_{RF-1} \cdot \tau}$$

, Eq. 19a-b

$$\frac{1}{\tau} \int_0^{\tau} \text{Sin}((2n-1) \cdot (2\pi \cdot f_{RF-1} \cdot t_{RF-1} + \xi_{RF-1})) dt =$$

$$\frac{\text{Sin}(2 \cdot n \cdot (\xi_{RF-1} + \pi \cdot f_{RF-1} \cdot \tau)) \cdot \text{Sin}(2 \cdot n \cdot \pi \cdot f_{RF-1} \cdot \tau)}{2 \cdot n \cdot \pi \cdot f_{RF-1} \cdot \tau}$$

Thus, the higher order Bessel functions will independently go to zero, regardless of the random phase terms, when

$$f_{RF-1} \cdot \tau = m \tag{Eq. 20}$$

where m is a positive integer. By using a phase modulator, setting the phase modulation amplitude,  $\beta$  equal to a zero of  $J_0$ , and setting product of the phase modulation frequency times the integration time (often the pulse duration) equal to a positive integer, all of the terms in Eq. 17 are zero, giving perfect apparent incoherence with an ACF equal to zero.

As stated previously, excellent incoherence can also be achieved if  $f_{RF-1} \gg 1/\tau$ , in that case the residual amplitude of the interference can be reduced significantly, and for some applications that approach may be sufficient. Through careful inspection, however, we find that modulation frequencies much faster than detector integration time are not necessary. For example, if the pulsed system described above employs a source with 1 ns pulses, a modulation frequency of 1 GHz is sufficient to drive the ACF to zero.

Finally, in practice it is not necessary for the ACF to be zero in many cases an upper limit of 0.5 may be acceptable. Therefore, the exact phase modulation amplitudes and the exact phase modulation frequencies listed can be varied and evaluated using Eq. 12 to calculate the worst case ACF for the system of interest. While the example above was analyzed for a square pulse, it is also possible to adjust the phase modulation frequencies to provide excellent cancellation of the interference for other pulse shapes.

In the more general case for arbitrary pulse shapes and non-ideal values of  $\beta$  and  $f_{RF-1} \tau$ , it is only necessary that  $ACF_{design}$  be reduced to an acceptable level for the application of interest, that is

$$ACF_{design} \leq ACF_{max} \quad ,Eq. 21$$

where  $\Delta I_{Ave\_max}$  represents the maximum allowable magnitude of the interference term in the combined beam. Therefore, in practice it is only necessary to adjust the phase modulation amplitude and the product of  $f_{RF-1} \tau$  so that,

$$ACF_{max} \geq \left[ \frac{\frac{1}{\tau} \left| \int_T^{T+\tau} A_1(t_1) A_2(t_2) \cdot \text{Cos}(\phi_0 + \beta_1 \cdot \text{Sin}[\omega_{RF-1} \cdot t_{RF-1} + \xi_{RF-1}]) \cdot dt \right|}{\frac{1}{\tau} \left| \int_T^{T+\tau} \left[ \frac{A_1^2(t_1) + A_2^2(t_2)}{2} \right] \cdot dt \right|} \right], Eq. 23$$

for any arbitrary  $\phi_0$  and  $\xi_{RF-1}$  to meet the required intensity variation specification for the application of interest.

### 2.3 Multiple Legs Phase Modulated

The apparent incoherence method can be applied to any number of legs, where the numbers of legs that can be combined are limited by the range of modulation frequencies that are possible with the phase modulators used in the implementation. For optimum performance each leg, should be phase modulated with the modulation amplitude in each leg should be equal to a zero of the Bessel function of the first kind of order zero. The design of a multiple leg system, including the two leg system with two phase modulators, is accomplished by adjusting the phase modulation amplitudes,  $\beta_i$ 's and the modulation frequencies,  $\omega_{RF-i}$ 's and the integration time,  $\tau$  to reduce the  $ACF_{max}$  to be less than the maximum acceptable,  $ACF_{design}$ , for the application of interest. An upper limit on the ACF can be calculated for a given set of  $\beta_i$ 's,  $\omega_{RF-i}$ 's and  $\tau$  by evaluating Eq. 12 ,

$$ACF = \left| \frac{\frac{1}{\tau} \int_T^{T+\tau} \left[ \sum_{i=1}^N \sum_{j=i+1}^N \left[ A_i(t_i) A_j(t_j) \cdot \text{Cos} \left( \begin{array}{l} \phi_{j0} - \phi_{i0} + \beta_i \cdot \text{Sin}[\omega_{RF-i} \cdot t_{RF-i} + \xi_{RF-i}] \\ -\beta_j \cdot \text{Sin}[\omega_{RF-j} \cdot t_{RF-j} + \xi_{RF-j}] \end{array} \right) \right] \right] \cdot dt}{\int_T^{T+\tau} \sum_{i=1}^N \left[ \frac{A_i(t_i)^2}{2} \right] \cdot dt} \right|, \text{Eq.12}$$

for a given set of experimental parameters can be determined by evaluating Eq. 14 for all possible values of optical and RF phases and noting the maximum value of the ACF as the phases are varied,  $ACF_{max}$ . Then as long as  $ACF_{max} \leq ACF_{design}$  that set of parameters will not exceed the design specification. Note that while optimum performance may be achieved with the phase modulation amplitudes set equal to a zero of the Bessel function of the first kind of order zero, in practice the specified performance may be achieved at other phase modulation selections.

### 3.0 Experimental Results

Experimental results were obtained to verify the apparent incoherence method. The intensity interference of a single pulse from a two leg system, where one leg is modulated, is measured. The ACF metric, defined in Eq 13 is used to compare measured images and theoretical data.

A theoretical curve is generated by plotting ACF, Eq 15. The modulation amplitude is set at,  $\beta = 2.40$ . This is consistent with the first zero of the zero order Bessel function of the first kind. The phase fluctuations  $\phi_{10}$  and  $\phi_{20}$  are allowed to changes randomly from pulse to pulse, as well as the frequency modulator starting phase  $\xi_{RF-1}$ . ACF is calculated for a large number of pulses at a specific modulation frequency, e.g. 300, and the largest value of ACF is kept and plotted in the theory curve. This operation is repeated for a range of frequencies,  $\omega_{RF-1} = [0, \dots, \frac{2.15}{T}]$ , where T is the pulse duration.

The experimental images were taken with a triggered camera, such that one pulse is captured during the integration time of the detector. The captured image is the intensity time averaged over the pulse duration. The random phase fluctuations in the ACF calculation are accommodated by a changing optical path length consistent with any non-stabilized bench top setup. The starting phase of the modulation is also left to be random. ACF is calculated using Eq 15. Figure 5 below is a plot of the theoretical curve and typical experimental data.

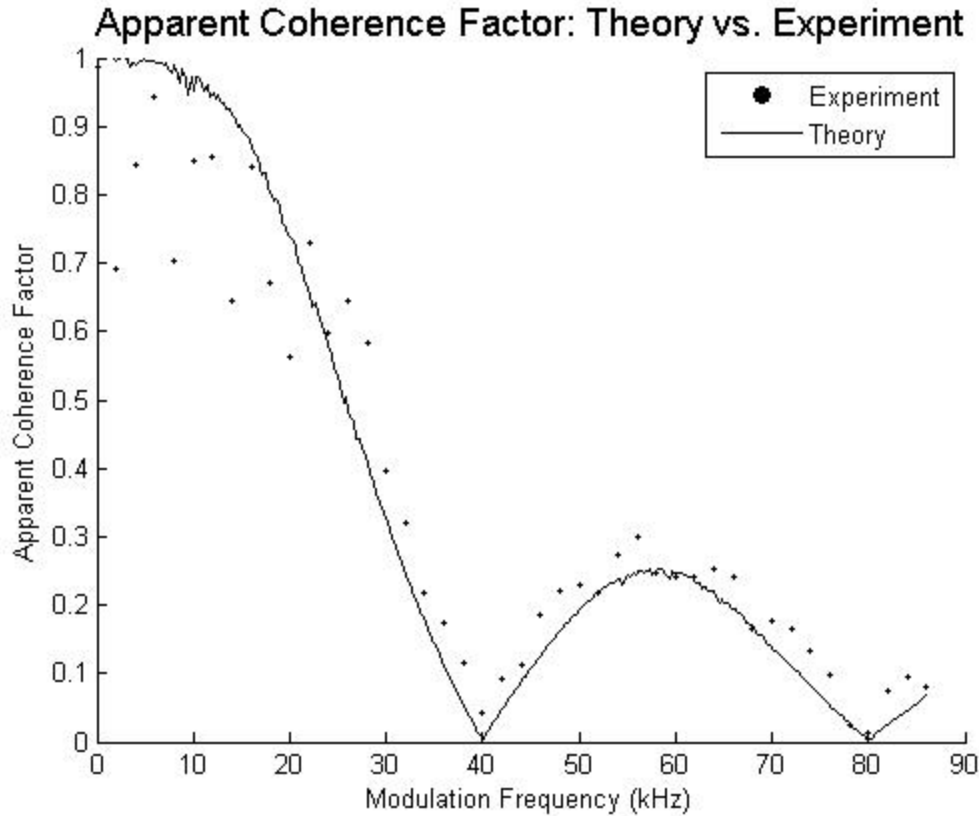


Figure 5: Apparent coherence factor vs. experiment for a pulsed fiber system with pulse duration of 25  $\mu$ sec.

#### 4.0 Conclusion

We have demonstrated the incoherent combination of a pulsed laser system with specific application to free space optical communications. The effect of sweeping interference fringes, caused by scintillation, across a detector decreases the likelihood of signal intensity fluctuations at the optical receiver. In this experiment we demonstrate a successful result for 25 $\mu$ sec pulses at a very low PRF. However, COTS LiNbO phase modulators with modulation capabilities in excess of 20 GHz are readily available allowing for this technique to be used in the nanosecond pulse regime.

- [1] Toshiaki Iwai, Toshimitsu Asakura, "Speckle Reduction in Coherent Information Processing," *Proceedings of the IEEE*, 84, , 765-781 (1996).
- [2] D.J. De Bitetto, "On the use of moving scatters in conventional holography," *Appl. Phys. Lett.* 8, 4 78-80. (1966)
- [3] Lai, Mig, "Speckle free laser probe beam," *Proceedings of SPIE*, 4996 (2003)
- [4] N. George and A. Jain, "Speckle reduction using multiple tones of illumination," *Appl. Opt.*, 12, 6 1202-1212, (1973)
- [5] B. Dingel and S. Kawata, "Speckle-free image in a laser-diode microscope by using the optical feedback effect," *Opt. Lett.* 18, 7 549-551 (1993)
- [6] J.C. Dainty and W.T. Welford, "Reduction of speckle in image plane hologram reconstruction by moving pupils," *Opt. Commun.*, 3, 289-294 (1971).
- [7] Y. Kawagoe, N. Takai, and T. Asakura, "Speckle reduction by a rotating aperture at the Fourier transform plane," *Opt. Lasers in Eng.*, 3 197-218, (1982)
- [8] T. Iwai, N. Takai and T. Asakura, "The autocorrelation function of the speckle intensity fluctuation integrated spatially by a detecting aperture of finite size," *Optica Atica*, 28, 10 1425-1437 (1981)
- [9] J. H. Churnside, "Aperture averaging of optical scintillations in the turbulent atmosphere," *Appl. Opt.* 30, 1982-1994 (1991)
- [10] Anguita, et al., "Multibeam space-time coded systems for optical atmospheric channels," *Proceedings of SPIE* , 6304-50, (2006).
- [12] E.M. Barja,\_, M. Afifia, A.A. Idrissia, K. Nassimb, S. Rachafib, "Speckle correlation fringes denoising using stationary wavelet transform. Application in the wavelet phase evaluation technique," *Optics & Laser Technology* 38, 7 506-511 (2006)
- [11]Khandekar et al., "Mitigation of dynamic wavefront distortions using a modified simplex optimization," *Proceedings of SPIE*, [6304](#)-58 (2006)

## DISTRIBUTION LIST

DTIC/OCP

8725 John J. Kingman Rd, Suite 0944

Ft Belvoir, VA 22060-6218 1 cys

AFRL/RVIL

Kirtland AFB, NM 87117-5776 2 cys

Official Record Copy

AFRL/RDLO/Michael L. Vigil 2 cys